Research article

Myocardial deformation characteristics assessed by cardiovascular magnetic resonance feature tracking in a healthy Chinese population

Huihui Kong [a], Jiaxin Cao [a], Lijun Zhang [b], Jing An [c], Xiaohua Wu [a,*], Yi He [a]

[a] *Department of Radiology, Beijing Friendship Hospital, Capital Medical University, Beijing, China*
[b] *Department of Radiology, Beijing Anzhen Hospital, Capital Medical University, Beijing, China*
[c] *Siemens Shenzhen Magnetic Resonance, MR Collaboration NE Asia, Shenzhen, China*

ABSTRACT

Purpose: To explore global/regional myocardial deformation across various layers, vascular distributions, specific levels and distinct walls in healthy individuals using cardiovascular magnetic resonance feature tracking (CMR-FT).

Methods: We selected a cohort of 55 healthy participants and CMR cine images were used to obtain the left ventricular (LV) peak longitudinal, circumferential, radial strains (LS, CS, RS). The characteristics of normal LV strain in various layers (endocardium, myocardium, epicardium), territories [left anterior descending artery (LAD), left circumflex artery (LCX), and right coronary artery (RCA)], levels (basal, middle, apical) and walls (anterior, septum, inferior, lateral) were compared.

Results: The absolute values of the LV global LS and CS gradually decreased from endocardium to epicardium. The absolute LV global RS ($65.7 \pm 47.7\%$) was maximum relative to LS ($-22.0 \pm 10.8\%$) and CS ($-22.8 \pm 7.7\%$). The absolute values of the LCX territorial strain were the largest compared with the LAD and RCA territorial strains. Regional RS, endo-CS and *endo*-LS gradually increased from the basal to the apical level. The LV lateral walls had the highest strain values (CS, LS, and RS).

Conclusions: Variations in normal LV strain values across various layers, territories, levels, and walls were observed, suggesting the necessity for careful clinical interpretation of these strain values. These findings also partially revealed the complexity of normal cardiac mechanics.

1. Introduction

The assessment of left ventricular (LV) motion function including systolic and diastolic functions, is the primary objective of a cardiac imaging study [1,2]. However, the global parameters commonly used in clinical practice, such as left ventricular ejection fraction (LVEF), are not sufficiently sensitive to detect subtle anomalies in LV function, indicating an early stage of the disease [3,4]. Due to these limitations, alternative measures such as myocardial strain have gained attention. Myocardial strain (deformation) is defined as the relative change in myocardial fibers from end-systole to end-diastole [3,5]. It is measured in 3 principal directions (radial, circumferential, and longitudinal) following the distinct directions of myocardial deformation [1,6]. Several, studies have

confirmed the vital role of myocardial deformation in early diagnosis, differential diagnosis, and prognosis in patients with various cardiac diseases [7–11].

Echocardiography and computed tomography are used for assessing myocardial deformation. However, cardiovascular magnetic resonance (CMR) remains advantageous for widespread clinical applications because of its high spatial and contrast resolution, radiation-free characteristics, and noninvasive reference standard for assessing of cardiac anatomy and function [12,13]. Several proposed techniques for CMR strain analysis, such as myocardial tagging, displacement encoding and strain encoding require additional sequences and time, and hence are rarely used clinically [1,2,14]. CMR feature tracking (CMR-FT) is an emerging technique that allows the assessment of myocardial global/regional deformation and displacement parameters derived from routine, balanced steady state free precession (SSFP) cine images [1,15–17]. In the last decade, research hotspots have focused on analyzing CMR-FT normal reference values [15,18–22]. However, no studies to date have systematically characterized normal myocardial strain using CMR-FT, which is essential for the early diagnosis, treatment, and even prognosis of the disease.

Addressing this notable gap, our study aimed to systematically explore global/regional myocardial deformation patterns, including various layers, segments, and vascular distributions, in healthy participants. In this effort, we sought to establish a comprehensive baseline understanding of normal myocardial strain using CMR-FT. This is fundamental to unraveling the complexity of cardiac mechanics and enhancing the accuracy of clinical assessments in cardiac diseases.

2. Materials and methods

2.1. Population

From the CMR database, we selected a cohort of 55 healthy subjects (all CMR studies were performed between March 2016 and October 2023). The study inclusion criteria were as follows: (1) no prior diagnosis of various cardiomyopathy, chronic kidney disease, hypertension, diabetes mellitus or hyperlipidemia that cause an increased risk of cardiovascular disease; (2) no symptoms or prior history of cardiovascular or cerebrovascular disease; and (3) normal physical examination and electrocardiogram. The exclusion criteria were as follows: (1) abnormal cardiac dimensions and function on cine CMR; (2) definite defects on perfusion images or a delayed enhancement signal on late gadolinium enhancement (LGE) images of CMR; (3) myocardial diseases including primary and secondary cardiomyopathies, such as hypertrophic cardiomyopathy, dilated cardiomyopathy, and arrhythmogenic right ventricular cardiomyopathy; (4) congenital cardiac abnormalities including anomalous coronary arteries; and (5) images that could not be analyzed, including those after a failed imaging study and those with unacceptable image quality. Only CMR studies yielding a remarkable to excellent image quality were selected, as judged by an experienced reader with more than 10 years of CMR experience. All subjects were in sinus rhythm at the time of the CMR examination. The study protocol conformed to the Declaration of Helsinki, and the study was approved by the ethics committee of our hospital. All subjects provided written informed consent.

2.2. CMR protocol

Imaging was performed using a 3T magnetic resonance imaging (MRI) system (MAGNETOM Prisma, Siemens Healthcare, Erlangen, Germany) with an 18-channel body coil. We examined all CMR images of each participant to guarantee image availability. For CMR-FT post-processing, a balanced SSFP cine images were obtained during repeated breath-holds in 3 long-axis (2-, 3-, and 4-chamber) views and in short-axis views covering the LV. The imaging parameters were as follows: repetition time (TR)/echo time (TE) = 3.1 milliseconds/1.3 ms; flip angle (FA) = 55°; field of view (FOV) = 276 × 340 mm^2; matrix = 156 × 192; and slice thickness = 5 mm for the long axis and 8 mm for the short axis, with 25 cardiac phases.

For the perfusion and LGE sequences, gadolinium contrast (Magnevist, Bayer Healthcare, Berlin, Germany) was administered intravenously at an injection rate of 4 mL/s and dose of 0.05 mmol/kg, followed by a 20-mL saline flush in the right arm. The perfusion sequence was performed during every cardiac cycle, and the images were acquired in 3 short-axis (basal, mid, and apical) views and one 4-chamber view of the LV. The imaging parameters were as follows: TR/TE = 2.9 milliseconds/1.1 ms; FA = 12°; TI = 100 ms; FOV = 350 × 450 mm^2; and slice thickness = 8 mm.

LGE images were acquired 10–15 min post-contrast administration in the same planes as the cine images using a T1-weighted gradient-echo pulse sequence with a phase-sensitive inversion recovery reconstruction. The imaging parameters were as follows: TR/TE = 4.1 milliseconds/1.56 ms; FA = 20°; FOV = 350 × 284 mm^2; and slice thickness = 5 mm for the long-axis view and 8 mm for the short-axis view.

2.3. Imaging analysis

The LV functional parameters were analyzed using dedicated software (Argus, Siemens Healthcare, Erlangen, Germany). The following parameters were measured: LVEF, LV end-diastolic volume (LVEDV), LV end-systolic volume (LVESV), LV cardiac output (LVCO), and LV stroke volume (LVSV).

Two-dimensional strain analysis was performed by 2 experienced observers using Medis Suite software (Medis Medical Imaging BV, Leiden, The Netherlands). Manual contouring was performed on the end-diastolic frames of both long- and short-axis cine images to determine the LV endocardial and epicardial borders. Then, the contours were automatically propagated to all phases and modified manually, if necessary. The papillary muscles were excluded from the endocardial contour. The superior insertion point was subsequently labeled on the junction of the left and right anterior walls to identify 16 segments. In addition, the cine long-axis (2-, 3-, and 4-

chamber) images were used for analyzing LV peak longitudinal strain (LS), and cine short-axis images (basal, mid, and apical) were used for analyzing the LV peak circumferential strain (CS) and radial strain (RS) (Fig. 1). (1) The global strains, including global longitudinal, circumferential, and radial strains (GLS, GCS, and GRS), were software-generated and recorded. Also, the LV layer strains were labeled, including the subendocardial, mid-myocardial, and epicardial regional CS (endo-CS, myo-CS, and epi-CS); and the subendocardial, mid-myocardial, and epicardial regional LS (*endo*-LS, myo-LS, and epi-LS). (2) For the LV territorial strain. We defined the basal/mid-anterior and anteroseptal segments as well as the apical anterior and septal segments as the territory supplied by the left anterior descending artery (LAD) based on the AHA 16-segment model. The basal/mid-inferoseptal, inferior and the apical inferior segments were assigned to the right coronary artery (RCA) when it was dominant. The basal/mid-inferolateral, anterolateral and the apical lateral segments were generally assigned to the left circumflex artery (LCX) [23]. Finally, the territorial LS (TLS), RS (TRS), and CS (TCS) were recorded. (3) The LV regional strain was the peak of the phase mean of the corresponding segments at the 3 levels of LV including the basal level (S1–S6), middle level (S7–S12), and apical level (S13–S16). Further, the regional LS (RLS), regional CS (RCS), and regional RS (RRS) were recorded. (4) Finally, the LV strain on the anterior, septum, inferior, and lateral walls was determined.

2.4. Statistical analysis

The continuous variables were presented as means ± standard deviation (SD) or medians (interquartile range, IQR), and categorical variables as frequencies. The differences in LV strain values between multiple groups were assessed using one-way analysis of variance using post hoc t tests with Bonferroni correction. All statistical analyses were performed using SPSS version 26.0 (Statistical Package for the Social Sciences, International Business Machines, Inc., Armonk, NY, USA). P values of 0.05 or less indicated statistically significant differences.

3. Results

3.1. Study demographics

A total of 55 subjects (37 men, mean age 44.3 ± 13.7 years) with cine CMR images acceptable for CMR-FT analysis were recruited. Of these, 67% were male, with a mean age of 44 years, and 18 (33%) were female, with a mean age of 45 years. A summary of clinical characteristics and LV cardiac function is provided in Table 1.

3.2. Normal reference values for the LV global strain

The normal reference values for the LV global strain are depicted in Table 2 and Fig. 2. The normal reference values of the LV GLS and GCS and GRS were −22.0 ± 10.8% and −22.8 ± 7.7%. Notably, the absolute values of the LV GLS and GCS exhibited a gradual decrease from endocardium to epicardium, with significant variations observed across various layers (**P < 0.05**). In contrast, the radial
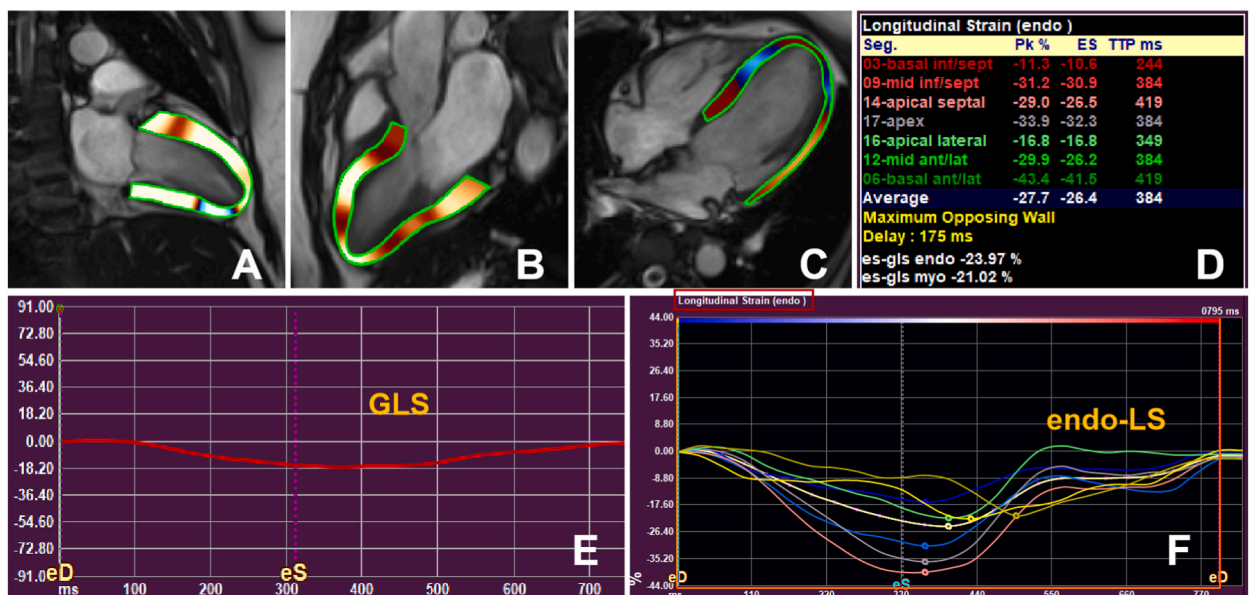

Fig. 1. Representative images in the standard long-axis (A–C) orientations and strain curves. Contours are illustrated in LV endocardial and epicardial borders in the 2-, 3-, and 4-chamber (A–C) views and corresponding LV GLS (E) and *endo*-LS (F). Peak systolic strain is provided for each myocardial segment (D).

Table 1

Baseline characteristics of the study cohort and cardiac function in the normal group.

	All (N = 55)	Male (N = 37)	Female (N = 18)
Baseline demographics			
Age (years)	44.3 ± 13.7	43.7 ± 12.8	45.4 ± 15.6
Weight (kg)	72.1 ± 13.3	75.3 ± 12.4	65.4 ± 12.8
Height (cm)	170.5 ± 8.1	173.9 ± 6.7	163.6 ± 6.2
BMI (kg/m^2)	24.8 ± 4.3	24.9 ± 3.7	24.6 ± 5.3
BSA (m^2)	1.8 ± 0.2	1.9 ± 0.2	1.7 ± 0.2
Rest HR (beats/min)	71.8 ± 12.5	71.7 ± 13.0	72.0 ± 11.8
Cardiac function			
EDV (mL)	119.8 ± 28.0	126.1 ± 29.4	107.0 ± 20.3
ESV (mL)	46.6 ± 14.4	50.2 ± 14.5	39.1 ± 11.0
SV (mL)	73.0 ± 18.5	75.4 ± 21.0	67.9 ± 10.7
EDV/BSA (mL/m^2)	65.0 ± 13.9	65.9 ± 14.6	63.1 ± 12.6
ESV/BSA (mL/m^2)	25.1 ± 6.9	26.2 ± 6.9	23.0 ± 6.4
SV/BSA (mL/m^2)	39.7 ± 9.8	39.5 ± 10.9	40.1 ± 7.2
CO (L/min)	5.2 ± 1.5	5.4 ± 1.6	4.9 ± 0.9
LVEF (%)	61.1 ± 6.8	59.7 ± 7.3	64.0 ± 4.7

Values presented as means ± SD or medians (IQR). BMI, body mass index; BSA, body surface area; CO, cardiac output; EDV, end diastolic volume; ESV, end systolic volume; HR, heart rate; LVEF, left ventricular ejection fraction; SV, stroke volume.

direction displayed less variation, resulting in the evaluation of the myocardial layer (Myo-GRS) at 65.7 ± 47.7%. Also, the absolute GRS was at the maximum relative to GLS and GCS at the same level.

3.3. Normal reference values for the LV territorial strain

The normal reference values for the LV territorial strain are provided in Table 3 and Fig. 3. The absolute values of the LCX territorial strain were the largest compared with the LAD and RCA, and the territorial strain values for various coronary distributions varied significantly (P < 0.05). For TRS, the absolute value of the LAD-territorial strain was higher than that of the RCA territorial strain. For TCS, the absolute value of the RCA territorial strain was higher than that of the LAD territorial strain (Table 3). The absolute value of TCS and TLS in the 3 coronary arteries (LAD, LCX, and RCA) decreased from endocardium to epicardium (Fig. 3).

3.4. Normal reference values for the LV regional strain

The normal reference values for the LV regional strain (basal, middle, and apical levels) are provided in Table 4 and Fig. 4. The regional strain from the base to the apical level gradually increased for myo-RRS, *endo*-RCS and *endo*-RLS. The regional strain from the base to the apical level gradually reduced for epi-RCS and epi-RLS (Table 4 and Fig. 4). The absolute value of RCS and RLS in the 3 levels (basal, middle, and apical) decreased from endocardium to epicardium.

3.5. Normal reference values for the LV strain on anterior, septum, inferior and lateral walls

The normal reference values for the LV strain on the anterior, septum, inferior and lateral walls are provided in Table 5 and Fig. 5. The LV CS and LS values decreased significantly on lateral, inferior, septum, and anterior walls (all P < 0.001). The LV lateral walls had the highest strain values (endo-CS, myo-CS, epi-CS, *endo*-LS, myo-LS, and epi-LS), with anterior walls having the lowest strain values. The LV RS values decreased considerably on lateral, anterior, inferior, and septum walls. The LV lateral walls had the highest strain values (80.5 ± 57.0%), with septum wall having the lowest strain value (46.4 ± 30.9%).

4. Discussion

This is a study to systematically characterized normal myocardial strain using CMR-FT, including various layers, walls, and vascular distributions, in a well-characterized group of healthy individuals. First, the absolute values of the LV GLS and GCS gradually decreased from endocardium to epicardium. Besides, the absolute GRS was maximum relative to GLS and GCS. Second, the absolute

Table 2

Normal reference values of the LV global strain.

Strain (%)	Global strain	LV-Endo	LV-Myo	LV-Epi	F	P value
GCS	−22.8 ± 7.7	−33.7 ± 10.9	−21.4 ± 8.0	−13.5 ± 7.5	1131.6	0.000
GLS	−22.0 ± 10.8	−23.6 ± 11.2	−21.8 ± 11.2	−20.6 ± 12.1	15.3	0.000
GRS	65.7 ± 47.7	–	65.7 ± 47.7	–	–	–

Values presented as means ± SD or medians (IQR). LV, left ventricular; GLS, global longitudinal strain; GCS, global circumferential strain; GRS, global radial strain.
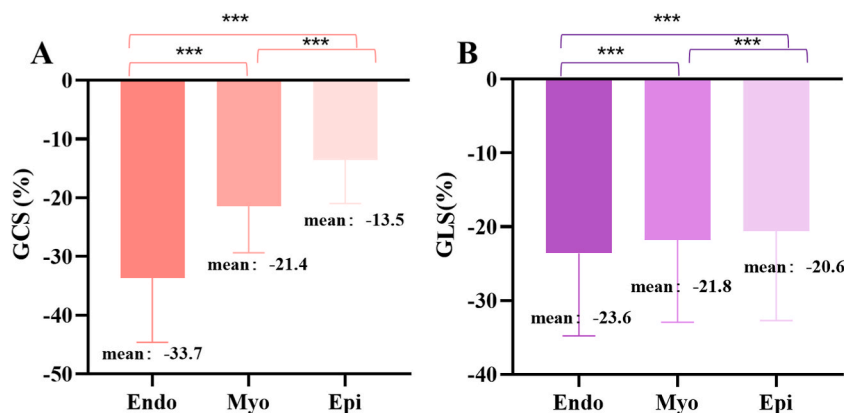
Fig. 2. Group comparisons of the LV layer-specific GLS/GCS in the normal group. The LV layer-specific GCS (*endo*-GCS, myo-GCS, and epi-GCS) in the normal group (A) and the LV layer-specific GLS (*endo*-GLS, myo-GLS, and epi-GLS) in the normal group (B). *** represents a statistically significant difference, namely, P < 0.05.

Table 3
Normal reference values of the LV territorial strain.

Strain (%)	LAD	LCX	RCA	F	P value
Endo-TCS	−31.8 ± 12.1	−35.8 ± 10.1	−33.7 ± 10.0	10.1	< 0.001
Myo-TCS	−18.2 ± 7.5	−24.8 ± 7.8	−21.8 ± 7.2	56.8	< 0.001
Epi-TCS	−10.3 ± 6.1	−17.0 ± 7.9	−13.8 ± 7.0	68.9	< 0.001
Endo-TLS	−22.9 ± 10.9	−25.4 ± 10.9	−22.6 ± 11.6	5.2	0.006
Myo-TLS	−20.7 ± 10.2	−23.9 ± 12.2	−21.0 ± 11.0	7.1	0.001
Epi-TLS	−19.3 ± 10.8	−22.9 ± 13.9	−19.9 ± 11.6	7.4	0.001
TRS	67.4 ± 45.9	80.5 ± 57.0	48.9 ± 31.8	32.6	< 0.001

Values presented as means ± SD or medians (IQR). LAD, left anterior descending artery; LCX, left circumflex artery; RCA, right coronary artery; TCS, territorial circumferential strain; TLS, territorial longitudinal strain; TRS, territorial radial strain.
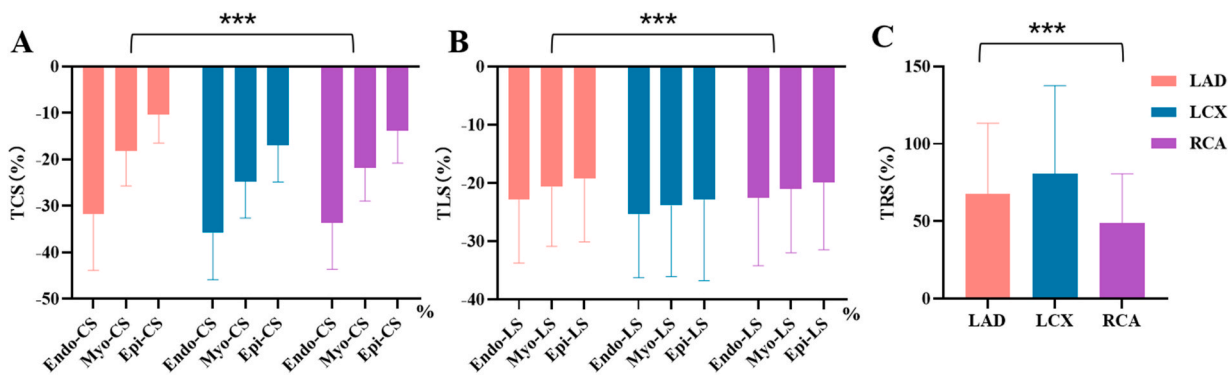

Fig. 3. Bar plots of the LV TLS/TCS/TRS in the normal group. The LV TCS (LAD, LCX and RCA territorial strains) in the normal group (A), the LV TLS (LAD, LCX and RCA territorial strains) in the normal group (B), and the LV TRS (LAD, LCX and RCA territorial strains) in the normal group (C). *** represents a statistically significant difference, namely, P < 0.05.

values of the LCX territorial strain were the largest compared with the LAD territorial and RCA territorial strains. Third, the regional strain from the base to the apical level gradually increased for RRS, *endo*-RCS and *endo*-RLS. Finally, the LV lateral walls had the highest strain values (CS, LS, and RS).

Many previous studies have indeed elucidated the normal strain values of LV [1,24,25], but none have studied the normal strain values of the coronary artery supply area, which is crucial for coronary heart disease. On the basis of studying the strain of different layers (basal, mid, apical) and different walls (subendocardial, mid-myocardial, epicardial), we also conducted strain analysis according to the distribution of coronary artery blood supply, including LCX, LAD, and RCA. The LV GLS and GCS values obtained in our study (GLS: −22% and GCS: −22.8%) were similar to the normal ranges obtained in a systematic review and meta-analysis [2]. This meta-analysis revealed FT-derived GLS and GCS values of −20.1% and −23%, which was concordant with our results. In particular,

Table 4
Normal reference values of the LV regional strain.

Strain (%)	Basal	Mid	Apical	F	P value
Endo-RCS	−33.1 ± 9.7	−32.0 ± 10.3	−37.0 ± 12.9	15.4	< 0.001
Myo-RCS	−22.1 ± 8.3	−20.3 ± 7.1	−21.4 ± 8.0	4.7	0.009
Epi-RCS	−15.1 ± 8.3	−12.6 ± 6.5	−12.4 ± 7.0	12.8	< 0.001
Endo-RLS	−21.8 ± 11.2	−24.1 ± 10.5	−25.5 ± 11.9	8.1	0.006
Myo-RLS	−22.3 ± 12.2	−22.2 ± 10.2	−20.2 ± 10.7	2.8	0.061
Epi-RLS	−22.8 ± 13.7	−21.0 ± 11.0	−16.6 ± 10.3	18.1	< 0.001
RRS	55.3 ± 39.4	66.1 ± 41.0	80.7 ± 62.3	19.5	< 0.001

Values presented as means ± SD or medians (IQR). RCS, regional circumferential strain; RLS, regional longitudinal strain; RRS, regional radial strain.
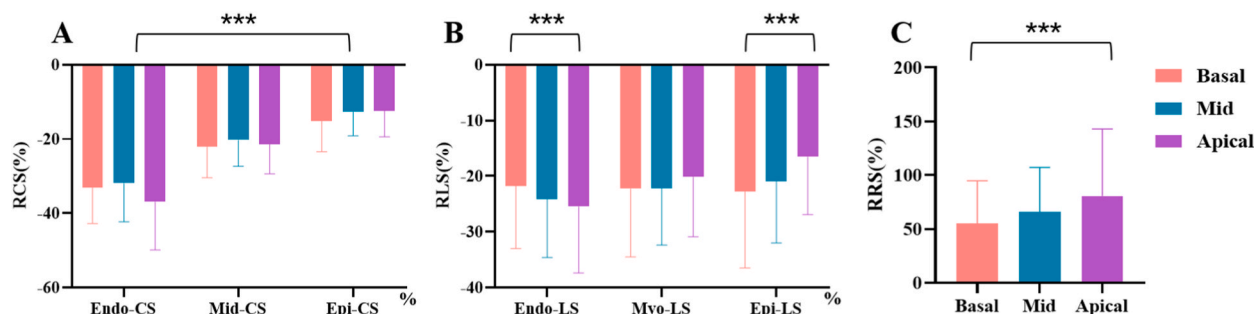

Fig. 4. Bar plots of the LV RLS/RCS/RRS in the normal group. The LV RCS (basal, middle, and apical levels) in the normal group (A), the LV RLS (basal, middle, and apical levels) in the normal group (B), and the LV RRS (basal, middle, and apical levels) in the normal group (C). *** represents a statistically significant difference, namely, P < 0.05.

Table 5
Normal reference values of the LV strain on the anterior, septum, inferior and lateral walls.

Strain (%)	Anterior	Septum	Inferior	Lateral	P value
CS	−19.4 ± 7.0	−22.1 ± 7.0	−22.5 ± 7.6	−25.8 ± 7.7	< 0.001
Endo-CS	−30.6 ± 11.7	−33.4 ± 10.8	−33.5 ± 11.3	−35.8 ± 10.1	< 0.001
Myo-CS	−17.6 ± 7.3	−20.5 ± 7.2	−21.1 ± 8.0	−24.8 ± 7.8	< 0.001
Epi-CS	−10.3 ± 6.1	−12.3 ± 6.7	−12.9 ± 6.9	−17.0 ± 7.9	< 0.001
LS	−19.9 ± 10.4	−21.7 ± 9.3	−21.1 ± 11.5	−24.0 ± 11.7	0.001
Endo-LS	−22.3 ± 11.7	−22.6 ± 10.1	−23.6 ± 12.6	−25.4 ± 10.9	0.010
Myo-LS	−19.7 ± 10.7	−21.5 ± 9.5	−20.9 ± 11.9	−23.9 ± 12.2	0.001
Epi-LS	−17.6 ± 11.1	−20.9 ± 10.6	−19.1 ± 12.0	−22.9 ± 13.8	< 0.001
RS	79.7 ± 53.1	46.4 ± 30.9	59.4 ± 33.4	80.5 ± 57.0	< 0.001

Values presented as means ± SD or medians (IQR). CS, circumferential strain; LS, longitudinal strain; RS, radial strain.
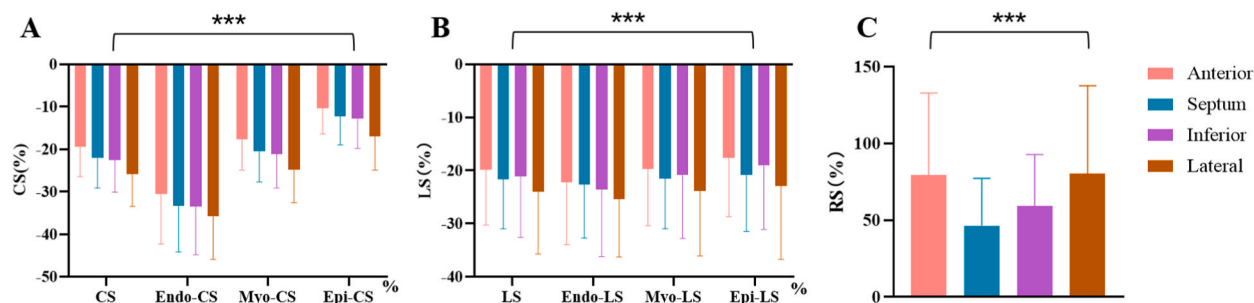

Fig. 5. Bar plots of the LV strain on the anterior, septum, inferior and lateral walls in the normal group. The LV CS (anterior, septum, inferior and lateral walls) in the normal group (A), the LV LS (anterior, septum, inferior and lateral walls) in the normal group (B), and the LV RS (anterior, septum, inferior and lateral walls) in the normal group (C). *** represents a statistically significant difference, namely, P < 0.05.

junping et al. [24] reported normal values of myocardial deformation in healthy Chinese individuals with GLS and GCS values of −22.4% and −24.3%, respectively, which was also consistent with our findings. Although the normal values of GLS and GCS were similar in multiple studies and fluctuated in a narrow range [1,2,24–26], GRS had a wide range. The GRS reported in our study (65.7%) was relatively greater than that reported in previous studies (34.1%) [2]. The meta-analysis of Vo et al. also failed to identify the source of this heterogeneity. We suggested 3 general reasons for this problem: (1) Normal strain values slightly varied among distinct populations [2]. Our results were in agreement with those of junping et al. [24](GRS 79%). This result further validated our hypothesis. (2) Various software used distinct algorithms (non-rigid algorithm or optical flow technology) for CMR-FT, ultimately leading to heterogeneity in results [19,20]. (3) Radial direction might be an influencing factor.

Our results indicated that the absolute values of the LV GLS and GCS gradually decreased from endocardium to epicardium (endocardium > myocardium > epicardium). This was because the myocardial motion was extremely complex, and the orientation of myofibers varied in distinct myocardial layers. The subepicardial myofibers contract through a left-handed helix and the sub-endocardial fibers are oriented in a right-handed helix. The middle-layer myocardial fibers move in a circumferential direction [27–29]. Our study only measured GRS, not divided into *endo*-RS and epi-RS. This was because the systolic strain (wall thickening) in the radial direction was in the order of millimeters. For example, when the end-diastolic myocardial thickness was 10 mm, and the systolic thickening reached 50%, the actual absolute change in myocardial thickness was only 5 mm. Based on the current spatial resolution of CMR cine imaging, the GRS assessment itself is extremely challenging, not to mention endo/epi-RS. In contrast, measuring changes from end-systole to end-diastole in the longitudinal and circumferential directions is easier [20].

A comprehensive understanding of the activation, contraction, and relaxation of the heart is complex and far beyond the ability of contemporary research. However, several previous studies have demonstrated remarkable efforts to explore and understand the myocardial structure and cardiac function [29–33]. As early as BC, humans recognized that the myocardium was a distinctive muscle that spreads the ventricular walls apart after each contraction [30–34]. Afterwards, Purkinje [32] confirmed that the apex of the heart remained motionless, whereas the atrioventricular junction moved toward and from it during ventricular systole and diastole. The ventricular myocardial fibers consisted of a single muscular band and contained 2 helices, the so-called right (basal loop, BL) and left ventricle (apical loop, AL) during its trajectory from the pulmonary artery to the aorta. The LV contained an ascending segment with fibers going up from the apex to the base and a descending segment with fibers coming down from the base to the apex. Furthermore, Hexeberg et al. [34] reported anisotropy in the thickness changes between various layers of the LV myocardium during contraction. He explained that the thickening of distinct muscle layers in the LV wall was not a reflection of the work by the fibers themselves in that layer because the thickening of the myocardial layer was not independent of other layers. Our study and previous studies demonstrated that LV architecture was much more complex. In the short-axis direction, the LV cavity had an oval rather than a circular configuration at the end-diastole. Moreover, in the long-axis direction, the LV wall flattened toward the apex. The LV wall gradually thinner toward the apex with the exception of the most basal level, composed of the membranous ventricular septum, due to the fibrous interventricular septum and the LV conical shape [33]. Thus, the myocardial movement pattern depended on the direction and spatial arrangement of the constituent muscular fibers. Besides, the differences in regional LV architecture and local stress, which led to an altered perfusion-related myocardial volume, might explain marked transmural gradients and regional inhomogeneities/heterogeneity of the LV myocardial strain.

Our study had some limitations. First, the research population was relatively small and it was a single center study. Afterwards, we will continue to include the population and expand the sample size to confirm our findings. Although a meta-analysis published by Yang et al. [35] in 2023 elaborated that different CMR-FT postprocessing software vendors would cause heterogeneity in strain values, but gender, age and CMR vendor had no effect on normal value measurements, we should also have a moderate proportion of men and women in follow-up studies. Second, there was a lack of other risk factors in this study, such as smoking, blood pressure, and alcohol consumption, and further research was needed on how they will affect strain values. Finally, left atrial deformation was excluded from this analysis, and the boundaries of the atrium were technically challenging due to their thin wall and potential morphological changes.

5. Conclusions

Our study showed the normal LV myocardial strain had transmural gradients and regional inhomogeneities/heterogeneity, which might help maintain the uniformity of fiber stress and strain during LV ejection and filling. When the aforementioned normal myocardial strain characteristics/transmural gradients were altered, it suggested adverse myocardial remodeling and LV dysfunction in the early stages of cardiac disease.

Ethics approval and consent to participate

The study protocol was approved by the Ethics Committee of Beijing Friendship Hospital (2021-P2-418-01). Written informed consent was obtained from the participants for publication of their individual details and images in this manuscript. All of the data and material are available.

Funding

Consent for publication

All the subjects provided written informed consent for the publication.

Data availability statement

We publish our data without reserve.

Declarations

Patients whose data or images are included in the publication have consented for all images and clinical data and other data included in the manuscript.

CRediT authorship contribution statement

Huihui Kong: Writing – original draft, Formal analysis, Data curation, Conceptualization. **Jiaxin Cao:** Project administration, Methodology, Investigation. **Lijun Zhang:** Supervision, Software, Resources. **Jing An:** Visualization, Supervision, Software. **Xiaohua Wu:** Writing – review & editing, Supervision, Conceptualization. **Yi He:** Writing – review & editing, Visualization, Resources, Conceptualization.

Declaration of competing interest

The authors declare that they have no known competing financial interests or personal relationships that could have appeared to influence the work reported in this paper.

References

[1] R.J. Taylor, W.E. Moody, F. Umar, et al., Myocardial strain measurement with feature-tracking cardiovascular magnetic resonance: normal values, Eur. Heart J. Cardiovasc. Imaging 16 (2015) 871–881.
[2] H.Q. Vo, T.H. Marwick, K. Negishi, MRI-derived myocardial strain measures in normal subjects, JACC Cardiovasc. Imaging 11 (2018) 196–205.
[3] J. Xu, W. Yang, S. Zhao, M. Lu, State-of-the-art myocardial strain by CMR feature tracking: clinical applications and future perspectives, Eur. Radiol. 32 (2022) 5424–5435.
[4] P. Claus, A.M.S. Omar, G. Pedrizzetti, P.P. Sengupta, E. Nagel, Tissue tracking technology for assessing cardiac mechanics: principles, normal values, and clinical applications, JACC Cardiovasc. Imaging 8 (2015) 1444–1460.
[5] J. Gorcsan 3rd, H. Tanaka, Echocardiographic assessment of myocardial strain, J. Am. Coll. Cardiol. 58 (2011) 1401–1413.
[6] F.A. Flachskampf, R. Blankstein, P.A. Grayburn, et al., Global longitudinal shortening: a positive step towards reducing confusion surrounding global longitudinal strain, JACC Cardiovasc. Imaging 12 (2019) 1566–1567.
[7] C. Schneeweis, J. Qiu, B. Schnackenburg, et al., Value of additional strain analysis with feature tracking in dobutamine stress cardiovascular magnetic resonance for detecting coronary artery disease, J. Cardiovasc. Magn. Reson. 16 (2014) 72.
[8] D.M. Vigneault, E. Yang, P.J. Jensen, et al., Left ventricular strain is abnormal in preclinical and overt hypertrophic cardiomyopathy: cardiac MR feature tracking, Radiology 290 (2019) 640–648.
[9] H.V. Lam, M. Groth, T. Mir, et al., Impact of chest wall deformity on cardiac function by CMR and feature-tracking strain analysis in paediatric patients with Marfan syndrome, Eur. Radiol. 31 (2021) 3973–3982.
[10] K. Fischer, S.J. Obrist, S.A. Erne, et al., Feature tracking myocardial strain incrementally improves prognostication in myocarditis beyond traditional CMR imaging features, JACC Cardiovasc. Imaging 13 (2020) 1891–1901.
[11] A.A. Kammerlander, C. Dona, C. Nitsche, et al., Feature tracking of global longitudinal strain by using cardiovascular MRI improves risk stratification in heart failure with preserved ejection fraction, Radiology 296 (2020) 290–298.
[12] A. Schuster, S. Kutty, A. Padiyath, et al., Cardiovascular magnetic resonance myocardial feature tracking detects quantitative wall motion during dobutamine stress, J. Cardiovasc. Magn. Reson. 13 (2011) 58.
[13] H. Rahman, C.M. Scannell, O.M. Demir, et al., High-resolution cardiac magnetic resonance imaging techniques for the identification of coronary microvascular dysfunction, JACC Cardiovasc. Imaging 14 (2021) 978–986.
[14] M.S. Amzulescu, M. De Craene, H. Langet, et al., Myocardial strain imaging: review of general principles, validation, and sources of discrepancies, Eur. Heart J. Cardiovasc. Imaging 20 (2019) 605–619.
[15] C. Lim, E. Blaszczyk, L. Riazy, et al., Quantification of myocardial strain assessed by cardiovascular magnetic resonance feature tracking in healthy subjects-influence of segmentation and analysis software, Eur. Radiol. 31 (2021) 3962–3972.
[16] A.M. Maceira, S.K. Prasad, M. Khan, D.J. Pennell, Normalized left ventricular systolic and diastolic function by steady state free precession cardiovascular magnetic resonance, J. Cardiovasc. Magn. Reson. 8 (2006) 417–426.
[17] K.N. Hor, R. Baumann, G. Pedrizzetti, et al., Magnetic resonance derived myocardial strain assessment using feature tracking, J. Vis. Exp. (2011), https://doi.org/10.3791/2356.
[18] B. Schmidt, A. Dick, M. Treutlein, et al., Intra- and inter-observer reproducibility of global and regional magnetic resonance feature tracking derived strain parameters of the left and right ventricle, Eur. J. Radiol. 89 (2017) 97–105.
[19] M. Barreiro-Perez, D. Curione, R. Symons, P. Claus, J.U. Voigt, J. Bogaert, Left ventricular global myocardial strain assessment comparing the reproducibility of four commercially available CMR-feature tracking algorithms, Eur. Radiol. 28 (2018) 5137–5147.
[20] M. Dobrovie, M. Barreiro-Perez, D. Curione, et al., Inter-vendor reproducibility and accuracy of segmental left ventricular strain measurements using CMR feature tracking, Eur. Radiol. 29 (2019) 6846–6857.
[21] V.T. Truong, C. Palmer, S. Wolking, et al., Normal left atrial strain and strain rate using cardiac magnetic resonance feature tracking in healthy volunteers, Eur. Heart J. Cardiovasc. Imaging 21 (2020) 446–453.
[22] Y.Y. Qu, J. Paul, H. Li, G.S. Ma, D. Buckert, V. Rasche, Left ventricular myocardial strain quantification with two- and three-dimensional cardiovascular magnetic resonance based tissue tracking, Quant. Imag. Med. Surg. 11 (2021) 1421–1436.
[23] M.D. Cerqueira, N.J. Weissman, V. Dilsizian, et al., Standardized myocardial segmentation and nomenclature for tomographic imaging of the heart, J. Cardiovasc. Magn. Reson. 4 (2002) 203–210.

[24] J. Peng, X. Zhao, L. Zhao, et al., Normal values of myocardial deformation assessed by cardiovascular magnetic resonance feature tracking in a healthy Chinese population: a multicenter study, Front. Physiol. 9 (2018) 1181.

[25] F. Andre, H. Steen, P. Matheis, et al., Age- and gender-related normal left ventricular deformation assessed by cardiovascular magnetic resonance feature tracking, J. Cardiovasc. Magn. Reson. 17 (2015) 25.

[26] P. Pierpaolo, S. Rolf, B.P. Manuel, et al., Left ventricular global myocardial strain assessment: are CMR feature-tracking algorithms useful in the clinical setting? Radiol. Med. 125 (2020) 444–450.

[27] M.Y. Jeung, P. Germain, P. Croisille, S. El ghannudi, C. Roy, A. Gangi, Myocardial tagging with MR imaging: overview of normal and pathologic findings, Radiographics 32 (2012) 1381–1398.

[28] P.S. Rajiah, K. Kalisz, J. Broncano, et al., Myocardial strain evaluation with cardiovascular MRI: physics, principles, and clinical applications, Radiographics 42 (2022) 968–990.

[29] X. Zhang, P. Haynes, K.S. Campbell, J.F. Wenk, Numerical evaluation of myofiber orientation and transmural contractile strength on left ventricular function, J. Biomech. Eng. 137 (2015) 044502.

[30] C.C. Moore, C.H. Lugo-Olivieri, E.R. McVeigh, E.A. Zerhouni, Three-dimensional systolic strain patterns in the normal human left ventricle: characterization with tagged MR imaging, Radiology 214 (2000) 453–466.

[31] J. Bogaert, F.E. Rademakers, Regional nonuniformity of normal adult human left ventricle, Am. J. Physiol. Heart Circ. Physiol. 280 (2001) H610–H620.

[32] F. Torrent-Guasp, M.J. Kocica, A. Corno, et al., Systolic ventricular filling, Eur. J. Cardio. Thorac. Surg. 25 (2004) 376–386.

[33] M.J. Gotte, T. Germans, I.K. Russel, et al., Myocardial strain and torsion quantified by cardiovascular magnetic resonance tissue tagging: studies in normal and impaired left ventricular function, J. Am. Coll. Cardiol. 48 (2006) 2002–2011.

[34] E. Hexeberg, D.C. Homans, R.J. Bache, Interpretation of systolic wall thickening. Can thickening of a discrete layer reflect fibre performance? Cardiovasc. Res. 29 (1995) 16–21.

[35] W. Yang, J. Xu, L. Zhu, et al., Myocardial strain measurements derived from MR feature-tracking: influence of sex, age, field strength, and vendor, JACC Cardiovasc. Imaging (2023), https://doi.org/10.1016/j.jcmg.2023.05.019.